Chapter 7

Mineralization: Evidence from Fission Track Thermochronology

Wanming Yuan and Ke Wang

Additional information is available at the end of the chapter

http://dx.doi.org/10.5772/intechopen.72277

Abstract

Ore deposits were the product of the Earth's material movement in a certain historical stage and tend to experience different forms and different degrees of change until being found, exploited and utilized. We should attach importance to conservation and changes of ore deposits besides metallogenic environment, ore deposit model and origin research. The conservation is closely related to uplifting and denudation so that to recover histories of uplifting and denudation for ore districts could reveal conservation and changes of mineral deposits. By applying fission track thermochronology, this chapter presents a research sample to discuss the issue, especially the relative technical method, and provides evidences for both deep ore prospecting and mineralizing potentiality evaluation. Meanwhile, dating mineralizing age is another frontier topic in the world. The author successfully applied fission track thermochronology to determining the mineralizing ages and epochs of the hydrothermal deposits. Steps and methods of achieving these goals are shown in detail. Geologists could take this chapter as a reference tool.

Keywords: mineralizing age, mineralizing epoch, preservation of orebody, tectonics, fission track thermochronology

1. Introduction

How to confirm mineralizing age and epoch of hydrothermal ore deposits is a frontier issue to research on mineralization in present-day world. The uncertainty of mineralization epoch highly restricts the deep research on the mineralization regularities, deposit origin, prospective prediction, and relationship between mineralization and tectonic thermal event. As a new technique method, fission track (FT) thermochronology has definite superiority for dating mineralizing age and epoch. We have a new significant attempt to apply the fission track

method to the hydrothermal mineralization. Since annealing of fission tracks occurs in crystal lattice and FT stability is hardly affected by other factors except temperature, the FT thermochronology is quite suitable for recording thermal events that take place in open system or enclosed system, in which the ore deposit formed. Reconstruction of thermal event history is a good quality of the fission track method that can indicate the variety relationship between temperature and time for the thermal event [1].

2. Fission track thermochronology

Silk and Barnes [2] first recognized track fading when they observed fission fragment tracks in muscovite mica under transmission electron microscope. Price and Walker [3] found the way to circumvent the problem of the rapid fading of tracks in muscovite mica and stabilized and fixed the tracks by chemical etching. They enlarged the tracks continuously by etching until the tracks were observed under optical microscope. Price and Walker [4] also discovered fossil tracks of ^{238}U spontaneous fission in muscovite mica and invented the technique of fission track dating. Fleischer et al. [5, 6] recognized that thermal fading of tracks follows the Arrhenius equation, and later many other scientists confirmed its correctness [7].

Fission track method has been widely used, and up to now, it is still one of basic techniques for nuclear science dating. In the basic dating formula,

$$t = \frac{1}{\lambda_D} \ln\left(\frac{\lambda_D N_F}{\lambda_F N_{238}} + 1\right) \tag{1}$$

^{238}U total decay constant $\lambda_D = 1.551 \times 10^{-10}a^{-1}$. The number of ^{238}U nuclei in spontaneous fission and that of existing N_{238} (number of existing ^{238}U nuclei) can be both accurately measured. Instead, no unified value of ^{238}U spontaneous fission constant λ_F had not been obtained till now [8], that is, λ_F values obtained by various laboratories via different methods, deviate greatly from one another. Now the three λ_F values used are indicated respectively: $(7.03 \pm 0.11) \times 10^{-17}a^{-1}$; $6.9 \times 10^{-17}a^{-1}$; $8.46 \times 10^{-17}a^{-1}$. The difference between the max and min values was large as 18.4%. When these two were inserted into Eq. (1) to calculate the age (order of 106a), they showed a difference of 18% or so. As a very complicated process, measuring N_F, that is, number of ^{238}U nuclei via chemical etching led to a high degree of uncertainty [9].

(U-Th)/He geochronology is a dating method that developed rapidly in recent years. Now this method has been widely used in crustal denudation research, near-surface substance dating and low-temperature geothermal history [10–12]. One of most important works in this technique is how to accurately determine ^{238}U, ^{232}Th, ^{147}Sm and ^{4}He contents in the mineral. Of all, neutron activation analysis (NAA) for ^{238}U, ^{232}Th and ^{147}Sm is a very advanced one. Instead, helium isotope, as a gas, makes itself difficult to measure. Based on the determination of solid-state nuclear track in apatite via thermal analysis method [13–15], the same method was employed to determine ^{4}He in apatite. This trial determination of the geological age got initial results. Here we expected this could give a reference for other scholars or inspire them.

Evidence for determination of geological age of apatite was supplied by the thermal analysis method.

The basic formula for (U-Th)/He dating is

$$N_{^4He} = 8N_{^{238}U}(e^{\lambda 238^t} - 1) + 7N_{^{235}U}(e^{\lambda 235^t} - 1) + 6N_{^{232}Th}(e^{\lambda 232^t} - 1) + 1N_{^{147}Sm}(e^{\lambda 147^t} - 1) \quad (2)$$

$N_{^4He}$, $N_{^{238}U}$, $N_{^{235}U}$, $N_{^{232}Th}$ and $N_{^{147}Sm}$ denote the numbers of ^{238}U, ^{235}U, ^{232}Th and ^{147}Sm nuclei, respectively; λ_{238}, λ_{235}, λ_{232} and λ_{147} are their respective α radioactive decay constants; t denotes the geological age of (U-Th)/He [15].

After crushing, grinding and sieving of the samples, apatites and zircons were concentrated and then separated using conventional magnetic and heavy-liquid methods. The zircon grains were mounted in glass slides, heated and covered by FEP Teflon sheets. Their external prismatic surfaces were ground and polished. Etching duration was about 20–35 h with NaOH/KOH(=1: 1) eutectic etchant at 210°C. Apatite was mounted in epoxy resin on glass slides and polished to expose internal grain surface. Spontaneous tracks were revealed by 5.5 N HNO_3 for 20 s at 21°C. Thin low-uranium muscovites as external detectors were packed together with sample grain mounts and CN2 as well as CN5 uranium dosimeter glass [16] irradiated and then etched in 40% HF for 20 min at 25°C to reveal the induced fission tracks.

Track densities for both natural and induced fission track populations were measured in air at 1000× magnification. The acceptable crystals for analysis should be prismatic sections parallel to the c-crystallographic axis. The track lengths were measured up to ~100 for each sample. Based on the IUGS-recommended Zeta calibration approach [17, 18] the fission track central ages were calculated. Errors were calculated using the techniques of Green. The χ^2 test is used to detect the probability that all age grains analyzed belong to a single population of ages [19]. A probability of <5% is evidence of an asymmetric spread of single-grain ages [20].

3. Metallotectonic event

Metallotectonic event is an important side of ore deposit research. Most mineralizations are closely related to tectonic activities, especially hydrothermal mineralization. Metallotectonics generally control ore-fluid or ore-forming material migratory concentration and ore-body location. The FT thermochronology could play a significant role in this field. Stability of fission tracks is mainly correlated to temperature. Closure temperature of apatite fission tracks (AFT) is about 100°C [21]. If the apatites are subsequently heated over the closure temperature, the tracks will be annealed. Fission tracks will form again when the temperature drops under 100°C. Since the effect of geothermal gradient, the fission track of sample in the deep (>100°C) is generally annealed and the AFT age becomes zero [22].

The metallotectonic event evolution usually corresponds with mineralizing process. Almost all fission track ages are significantly lower than their host rocks since the low annealing temperature. These age grains analyzed could belong to a single population of ages, and so the samples experienced a thermal event, which resulted in complete annealing of the original tracks subsequent to the formation of their host rocks [23, 24]. The FT ages are directly related to the distances from the fault zone. The deep part with lower age near the fault zone uplifts

into the present surface because of a higher uplifting rate near the fault zone than distant from it. Although the samples were collected at similar elevation, the samples far from the fault zone display higher FT ages than those near the fault zone, since there is a higher geothermal gradient near the fault zone [25, 26].

4. Mineralization age and epoch

The FT technique method could provide information about both mineralizing ages and epochs, play a role of a geological thermometer that shows a continuous variety of relationship between temperature and time and hence constrain on the thermal history of mineralizing thermal event. The FT thermochronology has been applied to recovery of the geological thermal history widely more and more at home and abroad [27, 28].

The hydrothermal mineralizing temperature was lower, such as 100–300°C, and zircon and apatite fission tracks have the retention temperature of ~250 and ~100°C, respectively. Thus, the zircon and apatite fission track ages present the thermal event just after the mineralization. However, the polyperiodic magmatic activities and mineralization superimpositions were not only a dominant factor of huge metal accumulation but also the dynamical reason of polyperiodic long-duration mineralization [20].

The Jiapigou gold belt in the Jilin Province, northeast China, has been an important gold-producing area for more than about 190 years.

There is widespread evidence for hydrothermal alteration, and some of this may be associated with the younger intrusives, which are likely related to the arc that developed during the Mesozoic as the Mongolian seaway (paleo-Teths or paleo Okhotsk ocean) closed, and final consolidation took place between Siberia and the composite Sino-Korean-North China block. Related intrusives across the Jiapigou gold belt and surrounding areas include the large Huangnihe and Wudaoliuhe-Diaoshuihu bodies. The age of the pink moyite Wudaoliuhe-Diaoshuihu pluton, situated SE of the Jiapigou gold belt (**Figure 1**), which has an EW-trending ellipsoid shape and is 20 km long by 6 km wide, is unknown. Thus, the origin of the gold mineralization in the Jiapigou gold belt cannot be fully resolved without full knowledge of the emplacement ages and thermal history of the younger intrusives. To address this, we collected a suite of samples from across the Jiapigou gold belt at outcrop and from the mines and applied zircon geochronology, trace element analysis and fission track and argon thermochronometry.

4.1. Analytical results

4.1.1. Zircon U–Pb ages

The entire dataset, some 118 ages, yielded four age groups: 157–183, 200–213, 216–248 and 2342–2674 Ma (**Figure 2**). The youngest group of zircon U–Pb ages (166–170 or 157–183 Ma) correspond to the main early Yanshanian (Jurassic) period, the two intermediate groups of

http://dx.doi.org/10.5772/intechopen.72277

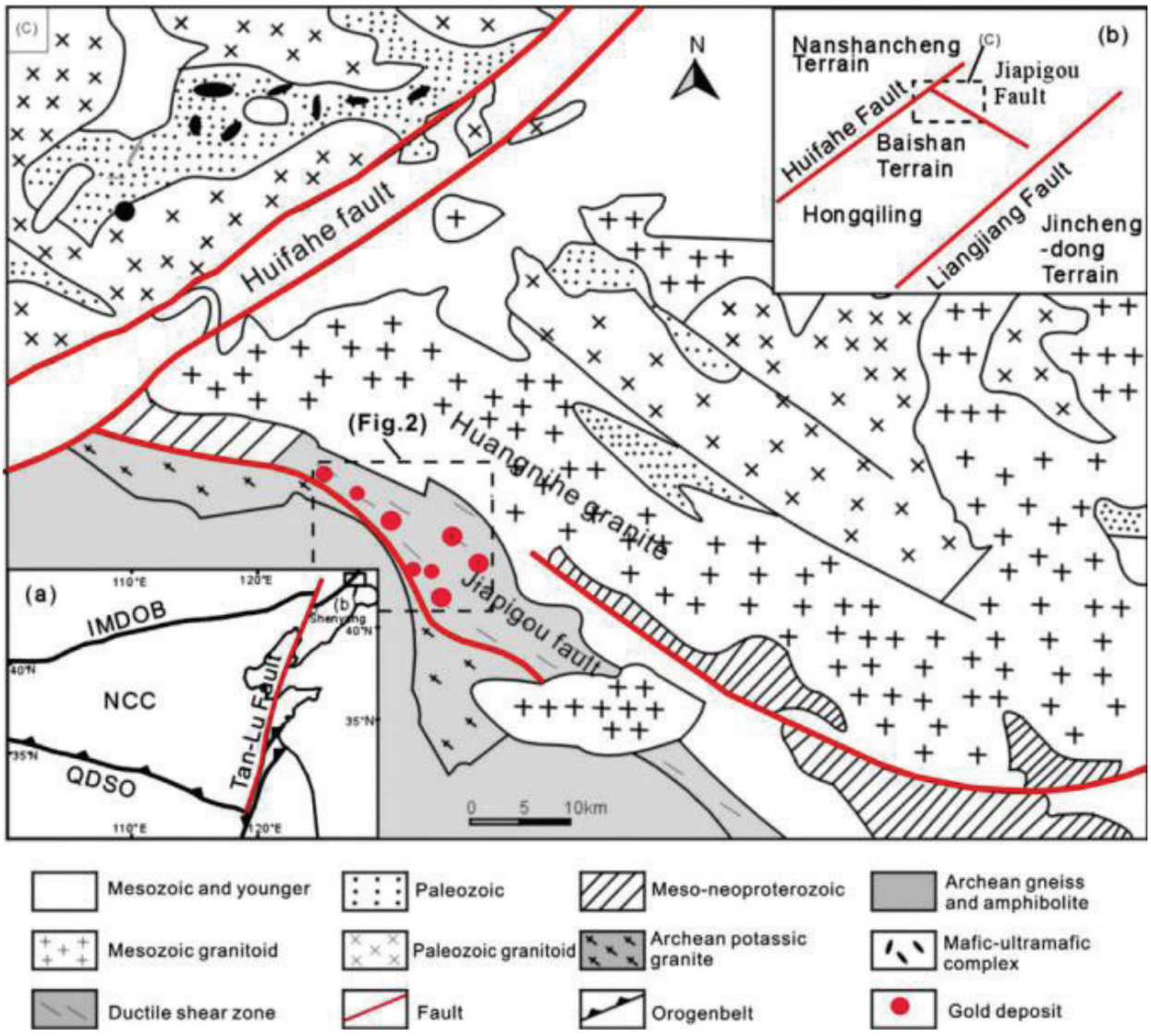

Figure 1. Geological map of the Jiapigou gold belt, eastern China. (a) Simplified map showing the location of the Jiapigou gold belt in the North China Craton (NCC) and adjacent orogenic belts, in which IMDOB is the inner Mongolian-Daxinganling orogenic belt and QDSO is Qinling-Dabie-Sulu orogen. (b) Simplified map showing the major regional faults and location of the Jiapigou gold belt. (c) General geology of the Jiapigou gold belt, showing the distribution of the major gold deposits.

zircon U–Pb ages (208 or 200–213 Ma; 228–230 or 216–248 Ma) correspond to the Indosinian (Triassic) period, and the oldest group of zircon U–Pb ages (2342–2536 or 2342–2674 Ma) correspond to the Paleoproterozoic.

4.1.2. Zircon fission track ages

Eleven samples were collected for ZFT analysis from different mine areas in the Jiapigou gold belt, and most of them are ore and altered rocks (**Table 1**). The results are given in **Table 1**. The central age range varies from 86 to 155 Ma. This wide age range represents various geological processes in the Jiapigou gold belt. The χ^2 test was used to examine the probability that ages

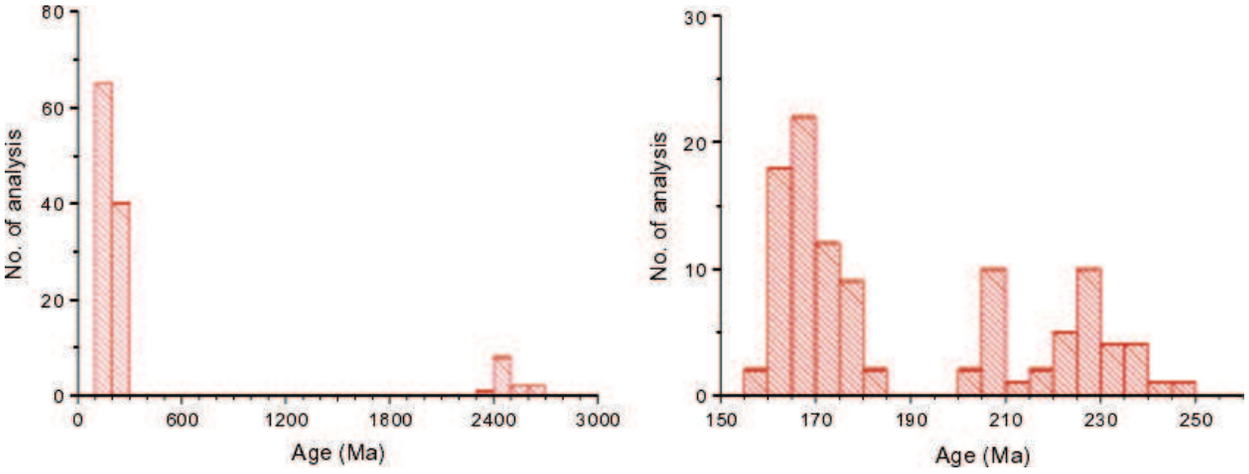

Figure 2. Histograms of the zircon U–Pb ages. Left—for all zircon grain ages; right—histogram for ages lower than 250 Ma.

obtained from zircon grains belong to a single population, using $\chi^2 > 5\%$ as statistical criterion [19]. A probability of <5% is evidence of an asymmetric spread of single-grain ages, indicating complex geneses and resources.

4.1.3. $^{40}Ar/^{39}Ar$ ages

All $^{40}Ar/^{39}Ar$ ages obtained from samples of K-feldspar and biotite as alteration minerals form age groups that are quite consistent with the groups of zircon U–Pb ages obtained from samples of magmatic rocks. Sample JP75 yielded an $^{40}Ar/^{39}Ar$ age for bioite of 228.9 ± 2.2 Ma and an $^{40}Ar/^{39}Ar$ age for K-feldspar of 217.5 ± 22.8 Ma that are similar to the zircon U–Pb age for granite of 229.8 ± 5.2 Ma. These indicate that not only K-feldspar and biotite in syenite were formed by the alteration but also that zircons in the same syenite were formed from the same metallogenic fluids that caused the formation of K-feldspar and biotite as alteration minerals. The $^{40}Ar/^{39}Ar$ plateau age of 170.3 ± 2.6 Ma for the JP88–2 K-feldspar sample denotes a younger alteration-mineralization episode that is consistent with the 170–166 Ma zircon U–Pb age group.

Among 11 samples subjected to ZFT analyses, eight samples have $P(\chi^2) > 5\%$, and three samples (BJ640-353-4-D, JP41-2, and JP100) have $P(\chi^2) < 5\%$ (**Table 1**); however, the amount of overdispersion (**Table 1**) is not large, and the pooled and central ages are the same.

The histogram of the combined ZFT data of convergent ages and decomposed divergent ages (**Figure 3**) shows three groups of ages: 86–106, 120–138 and 153–155 Ma. The number of samples increases from the highest age group to the lowest age group, which may mean enhancement of thermal event intensity from the Indosinian (Triassic) to Yanshan (Jurassic) epochs.

The bulk of the zircon U–Pb data and biotite $^{40}Ar/^{39}Ar$ age and K-feldspar $^{40}Ar/^{39}Ar$ ages obtained in this study relate to periods of alteration-mineralization in the Jiapigou gold belt. The zircon U–Pb ages indicate three periods of gold mineralization, that is, 230.0–228.9, 208.0 and 170.0–166.0 Ma. The biotite and K-feldspar $^{40}Ar/^{39}Ar$ ages of 228.9 ± 2.2 to 217.5 ± 22.8 Ma

Sample	Grains (N)	ϱ_s (10^5/cm^2) (Ns)	ϱ_i (10^5/cm^2) (Ni)	ϱ_d (10^5/cm^2) (Nd)	P(χ^2) (%)	Central age (Ma)	Pooled age (Ma)	U (ppm)
BJ640-353-4-D	16	161.621 (4655)	39.546 (1139)	6.069 (4630)	0.1	104 ± 7	105 ± 6	232.8
EDG1050-Tong-6-D	11	144.520 (3168)	30.063 (659)	6.136 (4630)	50.4	125 ± 8	125 ± 8	178.4
JL285-Zhu-13-D	9	115.404 (1384)	31.770 (381)	6.337 (4630)	13.6	98 ± 8	98 ± 7	184.1
JP100	22	167.633 (7234)	37.540 (1620)	6.605 (4630)	0.9	124 ± 8	125 ± 7	212
JP41-2	24	132.956 (7515)	33.880 (1915)	7.074 (4630)	4.5	117 ± 7	118±	175
JP54-01	23	100.335 (4892)	36.077 (1759)	7.275 (46.300)	90.8	86 ± 5	86 ± 5	182.4
JP78-2	7	164.513 (2167)	32.645 (430)	7.309 (4630)	80.6	155 ± 11	155 ± 11	166.5
JP79-2	17	140.135 (5455)	33.987 (1323)	7.175 (4630)	49	125 ± 7	125 ± 7	172.1
JXXT270-01-02	23	143.311 (6283)	39.528 (1733)	6.907 (4630)	6.5	106 ± 6	106 ± 6	206.8
JXXT270-02-04	18	161.681 (6103)	30.545 (1153)	6.852 (4630)	22.9	153 ± 9	153 ± 9	165.6
SDC740-115(100)-1D	21	141.684 (4039)	41.114 (1172)	6.789 (4630)	63.2	99 ± 6	99 ± 6	219.8

Notes: N, number of grains counted; ϱ_d, induced fission track density in muscovite external detectors over SRM; Nd, total number of fission tracks counted in ϱ_d; ϱ_i, induced fission track density in the muscovite external detector for crystals analyzed; Ni, total number of fission tracks counted in ϱ_i; ϱ_s, spontaneous fission track density on the internal surfaces of apatite crystals analyzed; Ns, total number of fission tracks counted in ϱ_s; P(χ^2), chi-squared probability that all single-crystal ages represent a single population of ages.

Table 1. Results of zircon fission track analyses.

and 197.9 ± 25.1 Ma correspond to the 230.0–228.9 Ma and 208.0 Ma zircon U–Pb ages of the two earlier periods of gold mineralization, respectively. The lower $^{40}Ar/^{39}Ar$ plateau age of 170.3 ± 2.6 Ma for JP88-2 K-feldspar sample is consistent with the 170.0–166.0 Ma zircon U–Pb age of the youngest period of gold mineralization.

Mineralized felsite and K-altered syenite gave the same zircon U–Pb ages of 228.9 ± 1.6 and 229.8 ± 2.0 Ma, respectively. A diabase dyke coexisting with auriferous quartz veins yielded a zircon U–Pb age of 230 ± 3.9 Ma. The age range, 228.9–230.0 Ma, could represent a period of gold metallogenesis because the samples are closely related to the gold mineralization in the Jiapiguo belt. Two other groups of zircon U–Pb ages—208 and 170–166 Ma obtained from hydrothermal zircons in a diabase dyke and granite bodies also reflect separate periods of gold metallogenesis. In view of all single grain ages obtained, the three groups of ages 248–216, 213–200 and 183–157 Ma indicate that episodes of gold metallogenesis in the Jiapiguo belt

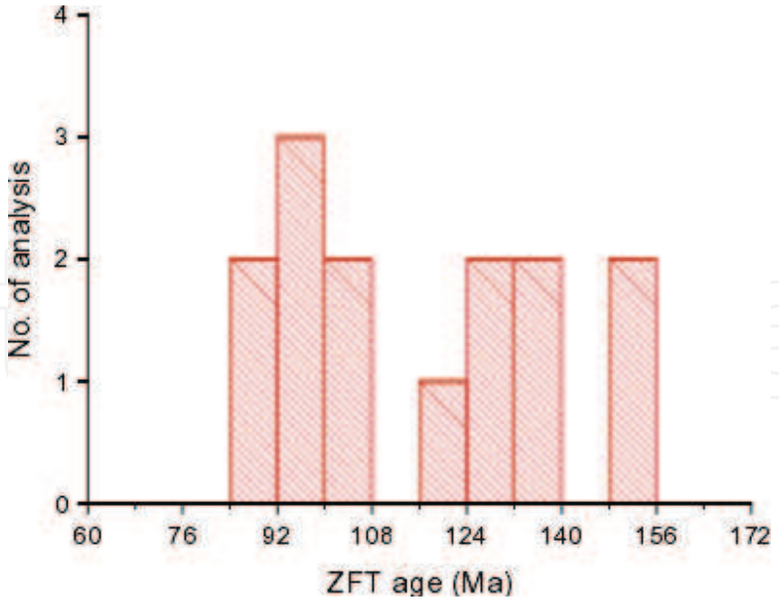

Figure 3. Histogram of zircon fission track (ZFT) ages obtained from ores from different deposits in the Jiapiguo gold belt. The three age groups of 86–106, 120–138 and 153–155 Ma indicate Indosinian and Yanshan epochs.

occurred during the Indosinian to Yanshanian epochs. However, some samples yielded old ages of 2342–2674 Ma, reflecting ore (metal) provenance from Precambrian rocks.

The obtained zircon fission track ages ranging from 86 ± 5 to 155 ± 11 Ma all fall into the Yanshanian epoch. According to distribution of the age data, these ages could be divided into three groups: 155–153, 138–120 and 106–88 Ma. Because zircon fission track age has a lower retention temperature than a corresponding zircon U–Pb age, the zircon fission track age group of 155–153 Ma likely corresponds to the zircon U–Pb age group of 170–166 Ma. The other two zircon fission track age groups-138-120 and 106–88 Ma likely represent younger periods of gold metallogenesis in the Jiapiguo belt.

Biotite from an altered host rock yielded a well-defined plateau $^{40}Ar/^{39}Ar$ age of 228.9 ± 2.2 Ma. K-feldspar from altered host rocks yielded total gas $^{40}Ar/^{39}Ar$ ages of 217.5 ± 22.8 and 197.9 ± 25.1 Ma, and another plateau $^{40}Ar/^{39}Ar$ age of 170.3 ± 2.6 Ma. These age data coincide well with the two older zircon U–Pb age groups mentioned above. Because altered minerals (biotite and K-feldspar) were formed during gold mineralization, their $^{40}Ar/^{39}Ar$ ages likely correspond to certain periods of gold metallogenesis in the Jiapiguo belt.

Therefore, the present age data obtained using three different methods reveal five periods of gold metallogenesis 230.0–228.9, 208, 170–153, 138–120 and 106–88 Ma in the Jiapiguo belt. The three middle groups of ages are the most likely plausible in view of the tectono-magmatic history of the North China Craton where the Jiapiguo and other gold belts in eastern China are situated. The multiple periods of gold metallogenesis in the Jiapigou belt were likely responsible for the formation of large gold deposits in the region, besides role of Precambrian rocks as plausible metal sources.

As a remarkable outcome of the present study, the multiple episodes of gold metallogenesis defined from the age data strongly correspond with ages of certain tectonic-magmatic events

that affected the northern margin of the North China Craton as reported from previous studies. Therefore, the age data obtained from zircon U–Pb dating, zircon fission track dating and $^{40}Ar/^{39}Ar$ dating in the present study reflect not only periods of gold metallogenesis but also periods of corresponding tectonic-magmatic activities that resulted in the super-large gold deposits in the Jiapiguo belt.

During the Indosinian epoch, gold mineralization in the Jiapugo belt can be associated with bidirectional continental subductions of the North China Craton due to its collision with the Angara Craton in the north and the Yangtze Craton in the south that resulted in continental oversteps and an evolutionary series of granitoids. The collision of the Siberia and Mongolia blocks with the North China Craton during Late Triassic-Early Jurassic (about 180–150 Ma) led to closure of the Mongolia-Okhotsk Ocean, inducing Cretaceous metallogenic processes nearly at the same time. The Late Yanshanian tectonic-magmatic-mineralizing events in the Jiapigou gold belt were mainly controlled by the subduction of the Pacific plate. The metallogenic episodes were contemporaneous with changes in a drift direction of the subducting Pacific plate. The subduction-related magmatisms, which were controlled by deep-seated regional faults (e.g., the NE-NNE-trending Tanlu Fault), mainly originated in the middle crust and/or near the Moho discontinuity from which ore-forming fluids were likely extracted [29].

5. Preservation of ore deposit

A useful approach is to use low-temperature thermochronology methods to constrain the unroofing/exhumation history of a region. In regions unaffected by extension, the primary process driving rock exhumation will be erosion. Take Harizha-Halongxiuma Cu-Mo polymetallic ore deposit for example, it is located in the eastern Central East Kunlun zone (**Figure 4b**). The East Kunlun Range is a complex lithospheric left-lateral strike-slip fault system that located in the northeastern Tibetan Plateau separating the Bayan Har-Songpan Ganzi to the south and the Qaidam basin to the north. Cu-Mo orebodies occur mainly with the granite porphyry, granitoid diorite and monzogranite. Some Cu ore bodies also occur in the contact zones and fracture zones.

5.1. Sample preparation and analytical technique

The collected rock samples were subjected to crushing, grinding and sieving. Both apatite and zircon concentrates were separated from the crushed rock samples using conventional magnetic and heavy-liquid separation techniques.

5.1.1. Age results

A total of six apatite and six zircon fission-track results were successfully completed for all the samples. In addition, two apatite (U-Th)/He ages were obtained. The results are presented in **Tables 2** and **3**. Samples with chisquare >5% means all grains in it formed within the same tectonic/thermal event. The apatite fission-track ages narrowly range from (102 ± 4) Ma to (87 ± 6) Ma with the mean track lengths ranging from (11.9 ± 2.3) μm to (12.6 ± 1.6) μm and the zircon

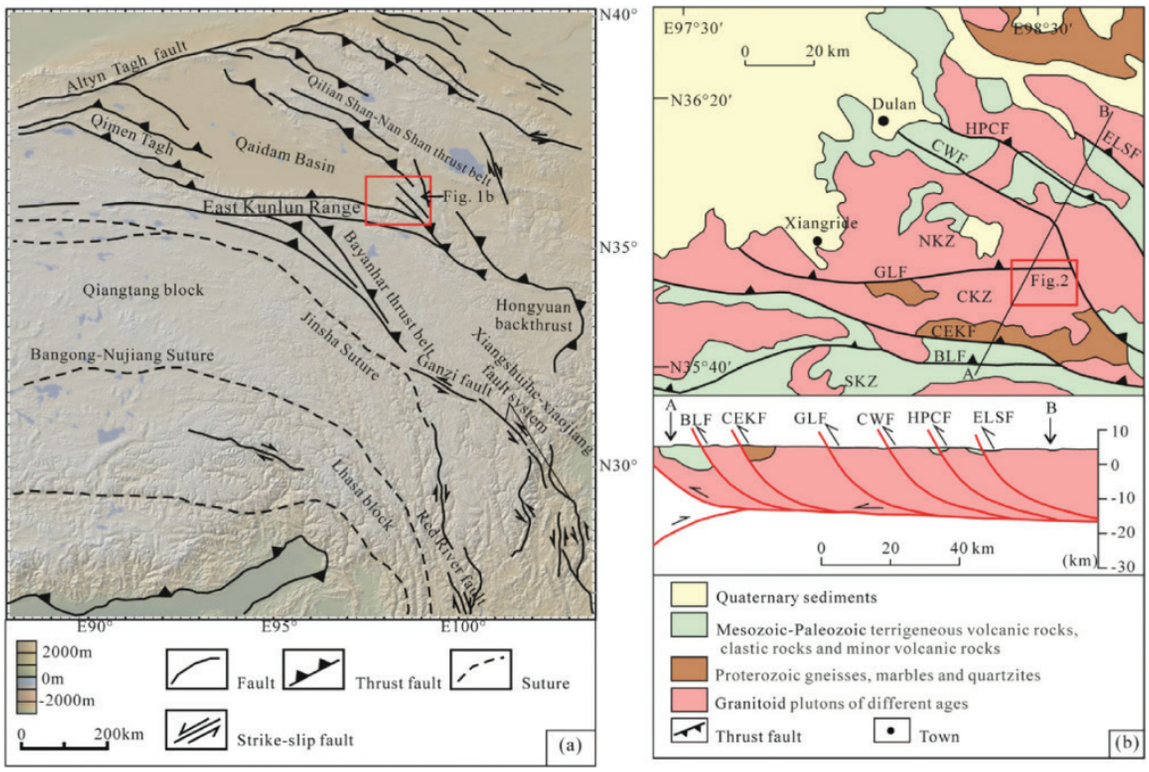

Figure 4. Map showing the location and geological setting of study area. (a) Map of the Tibetan plateau with main large-scale faults and terranes. (b) Sketch map of the eastern east Kunlun range, indicating the Elashan fault (ELSF), the Hacipu fault (HCPF), the Chahanwusu fault (CWF), the Goli fault (GLF), the central east Kunlun fault (CEKF) and the Boluoer fault (BLF). The section A-B is shown beneath the sketch map.

fission-track ages are ranging from (205 ± 14) Ma to (142 ± 7) Ma. The apatite (U-Th)/He dating test results of every grains provides a group of ages ranging from (68 ± 4.1) Ma to (52 ± 3.1) Ma with the mean ages of samples ranging from (60 ± 3.6) Ma to (56 ± 3.4) Ma.

5.1.2. Geothermal history

The HeFTy software [30] was used to model the thermal history based on the track length distribution and fission-track age data. Modeling of the fission-track data was based on our double dated samples with apatite and zircon fission-track dating. Time–temperature history was calculated using the annealing model of [31] and c-axis projected length [32]. The initial apatite fission-track length for this modeling was 16.3 μm. The modeling results are shown in **Figure 5**.

In **Figure 5**, all the temperature-time paths show a remarkable multi-stage pattern, including two rapid cooling stages and one relatively stable period in the Harizha-Halongxiuma ore deposit area since the Mesozoic. The time-temperature paths tend to be flat or have a low slope between approximately 100–60 Ma but become much more oblique before approximately 100 Ma and after approximately 60 Ma. The mean apatite (U-Th)/He ages are distributed around 60–56 Ma, which means that a remarkable decrease in temperature took place during the Paleocene. This is perfectly consistent with the thermal history in **Figure 5**. Besides

Sample/ mineral	Elevation	Rock type	n	No. of field of views	Spontaneous $\varrho_s(N_s)$	Induced $\varrho_i(N_i)$	Dosimeter $\varrho_d(N_d)$	P (χ^2) (%)	Central age (Ma) (± 1σ)	Mean track length (± 1σ)
XN12 + 15-Ap	4147	Crystal tuff	30	108	3.836(893)	8.583(1998)	11,682(8116)	98.7	102 ± 4	12.4 ± 1.9
XN12 + 15-Zr	4147	Crystal tuff	15		100.866(2102)	53.12(1107)	19.437(10030)	84.8	166 ± 9	
XN23-1-Ap	4358	Granite	30	101	3.641(958)	8.771(2308)	11.462(8116)	83.4	93 ± 6	12.4 ± 1.9
XN23-1-Zr	4358	Granite	27		112.321(3754)	75.908(2537)	21.385(10030)	83.9	142 ± 7	
XN26-Ap	4021	Quartz vein	30	101	3.973(1070)	10.563(2273)	11.02(8116)	68.0	101 ± 6	12.6 ± 1.6
XN26-Zr	4021	Quartz vein	8		181.112(1086)	91.556(549)	23.218(10030)	98.4	205 ± 14	
XN28-Ap	4094	Quartz vein	34	103	4.178(881)	10.126(2135)	10.8(8116)	96.5	87 ± 6	12.2 ± 1.7
XN28-Zr	4094	Quartz vein	7		169.125(1330)	88.377(695)	22.875(10030)	94.9	196 ± 12	
XN30-2-Ap	4138	Granite	28	102	4.074(1060)	8.555(2226)	10.579(8116)	83.8	98 ± 6	12.5 ± 1.9
XN30-2-Zr	4138	Granite	28		197.025(7166)	96.505(3510)	22.187(10030)	73.2	203 ± 9	
XN33-1-Ap	4069	Diorite	28	104	5.482(443)	11.782(952)	11.02(8116)	75.5	100 ± 8	11.9±2.3
XN33-1-Zr	4069	Diorite	28		181.299(6398)	93.257(3291)	21.843(10030)	44.4	190 ± 9	

Note: Track densities (ϱ) are as measured and are (10^5 per cm^{-2}); number of grains counted (n) are shown in parentheses. P(χ^2) is chi-square probability. Apatite ages calculated with ζ (zeta) = 392 ± 18.7 (yr cm^2/tr) and zircon ages calculated with ζ (zeta) = 90.9 ± 3.5 (yr cm^2/tr).

Table 2. Fission-track ages of apatite from the Harizha-Halongxiuma mine area using an external detector method and zeta calibration approach.

http://dx.doi.org/10.5772/intechopen.72277

Sample	He (nmol/g)	U (ppm)	Th (ppm)	Sm (ppm)	FT	He age (Ma)	Error
DL14-3_1	0.1452	5.1	17.6	105	0.66	68	4.1
DL14-3_2	0.1938	8.9	26.2	144	0.66	59	3.5
DL14-3_3	0.2424	11.3	42.0	177	0.65	52	3.1
Mean	0.1938	8.4	28.6	142.0	0.66	60	3.6
DL25 + 26_1	0.7024	11.7	38.3	171	0.74	56	3.4
DL25 + 26_2	0.5432	6.9	25.8	110.0	0.76	55	3.3
Mean	0.6228	18.6	32.1	141	0.75	56	3.4

Note: The estimated analytical uncertainty for He ages is about 6% (2σ).

Table 3. Apatite (U-Th)/He ages of Harizha-Halongxiuma mine area performed by furnace heating for He extraction and ICP-MS for U-Th determinations at the London Geochronology Centre.

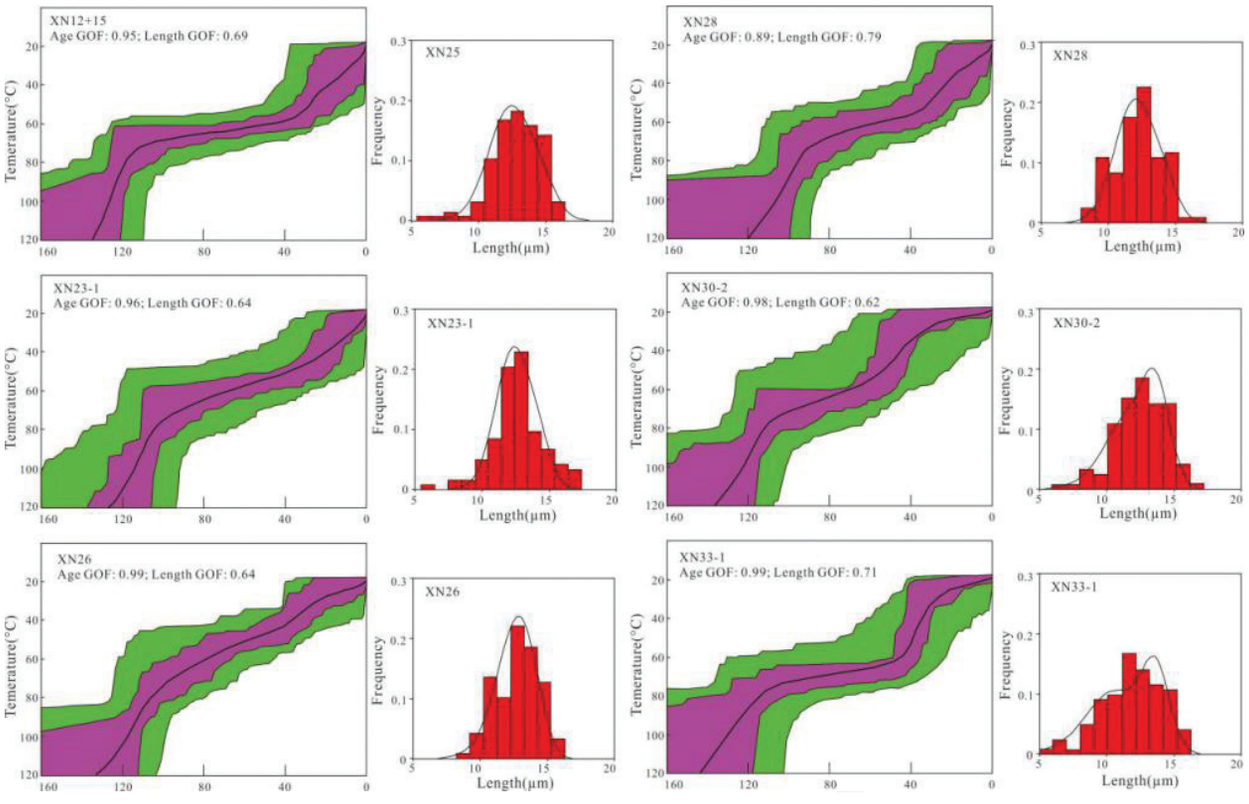

Figure 5. The inverse modeling results of samples in Harizha-Halongxiuma mine area. The time-temperature paths are modeled by the apatite fission-track data and distributions of apatite fission-track lengths with HeFty program by Ketcham [30]. The present day temperature is set as a constant value of 20°C. The dark gray area corresponds to the range of good fits, and the light gray area corresponds to the range of acceptable fits. The bold line in the dark gray area represents for the best modeled path. The Kolmogorov-Smirnov test was used to determine the goodness-of-fit of the solutions to the real data.

the temperature-time paths in **Figure 5**, the geothermal history with the temperature above 110°C can also be deduced. Thermal history with temperatures ranging between 210 and 110°C can be constrained by zircon and apatite fission-track ages because the temperature of samples

can be defined as zircon fission-track closure temperature when samples pass through the top of part annealing zone. Thus, samples in this chapter had undergone a rapid cooling stage after approximately 200 Ma.

Taking all the temperature–time paths and the apatite (U-Th)/He ages into consideration, we conclude the geothermal history of the Harizha-Halongxiuma ore deposit area as a three-stage pattern as follows: (1) the first rapid cooling stage during approximately 200–100 Ma; (2) a subsequent stable stage during approximately 100–60 Ma; and (3) the second rapid cooling stage after 60 Ma.

5.2. Discussion

5.2.1. Exhumational processes and mechanism

Thermal history should be consistent with the tectonic setting and geodynamics. The thermal history of Harizha-Halongxiuma ore deposit area should be mainly affected by a series of collisions and matching between different blocks of Tibet Plateau.

Our ZFT and AFT data obtained in Harizha-Halongxiuma mining area indicate a decrease of approximately 100°C (the closure temperature difference between the ZFT and AFT) in temperature between about 205–142 and 102–87 Ma with the amount of uplift-induced exhumation of 3.60 km. This large-scale uplift and uplift-induced exhumation during the Early-Middle Mesozoic was consistent with the transpressional thrust nappeing system in the East Kunlun Range.

As shown in **Figure 5**, the rapid cooling stage ended during about 120–100 Ma followed by the onset of a stable stage with relatively low cooling rate. The Neo-Tethys Ocean closed in about 60–40 Ma and the India plate started collide with Eurasian plate. Even though the collision initially took place on the southern edge of Tibet, the effect of the collision and subduction propagated northward and led to the large-scale uplift in the whole Tibetan Plateau. Correspondingly, both of the (U-Th)/He data and inversing modeling temperature-time paths in this chapter indicate that there is a rapid cooling event took place during 60–40 Ma and resulted in a large amount of uplift-induced exhumation in Cenozoic.

5.2.2. Preservation of the ore deposit

The Harizha ore deposit area underwent Mesozoic rapid cooling event and recorded ZFT ages much later than the Halongxiuma ore deposit area. As a result, the uplift-induced exhumation of each deposit area is also different since the Mesozoic. The ore bodies in Harizha-Halongxiuma ore deposit area have experienced a three-stage (230–100, 100–60 and 60–0 Ma) cooling path since the mineralization epoch with the cooling rates of 1.26, 0.50 and 1.50°C/Myr, respectively for each stage. Based on the geothermal gradient of 35°C/km, the amount of uplift-induced exhumation of each stage is 4.68, 0.57 and 2.57 km, respectively. The total amount of uplift-induced exhumation in study area is 7.82 km. Microthermometric studies of fluid inclusions in ore rock samples from study area revealed that the burial depth of ore deposits mineralization in the Harizha-Halongxiuma ore deposit area ranges from 6.5 to 8.6 km [33]. The fact that 7.82 km of exhumation is larger than the minimum burial depth of the ore deposit in Harizha-Halongxiuma ore deposit area indicates that the upper part of the ore bodies had already been partially denuded. Fortunately, the maximum burial depth of mineralization of

8.6 km is larger than the thickness of exhumation, which likely means that part of ore bodies are still buried under the Earth's surface. Generally, the exhumation thickness since the main mineralization epoch indicates that the ore bodies in Harizha-Halongxiuma ore deposit area have been nearly half eroded. Ore bodies of approximately 0.8 km in depth are still well preserved under the surface.

In Harizha-Halongxiuma mine area, the copper and molybdenum deposit belts are always observed as developing with/within the fracture zones. Y1-Y2 section was designed to discover the relationship between ore bodies and the host strata. Attention had been paid to define whether they had undergone the same denudation history. Based on our dating results and the modeling of temperature-time paths, sample XN12 + 15 started to experience Cenozoic rapid cooling in approximately 40 Ma but the apatite (U-Th)/He ages of DL14-3 shows a geothermal story of rapid cooling in about 68–52 Ma. Thus, the cooling onset of DL14-3 was clearly early than that of XN12 + 15. We infer that a thrusting movement happened in the Early Paleogene had brought DL14-3 from a much deeper layer, and the time was recorded by the helium due to high-rate exhumation. The ore bodies hosted in the Triassic strata were partially eroded along with the hanging wall (**Figure 6a**). For section X1-X2, four samples, such as XN26, XN28, XN30-2 and XN33-1, had undergone nearly the same exhumation history as their zircon and apatite fission-track ages fluctuated within a relatively narrow range. This indicates that the Permian–Triassic intrusions where the four samples were collected have undergone uniformed geothermal history and were exhumed to the Earth's surface together. In addition, the southwestward thrusting made the hangingwall underwent much thicker exhumation comparing with footwalls to the southwest (**Figure 6b**). The molybdenum mineralization was suggested to mainly form with/within the granitoid intrusions near the location of our samples. It is likely the rapid exhumation in Cenozoic that eroded the cover of the Mo-orebodies and made the orebodies outcropped on the Earth's surface.

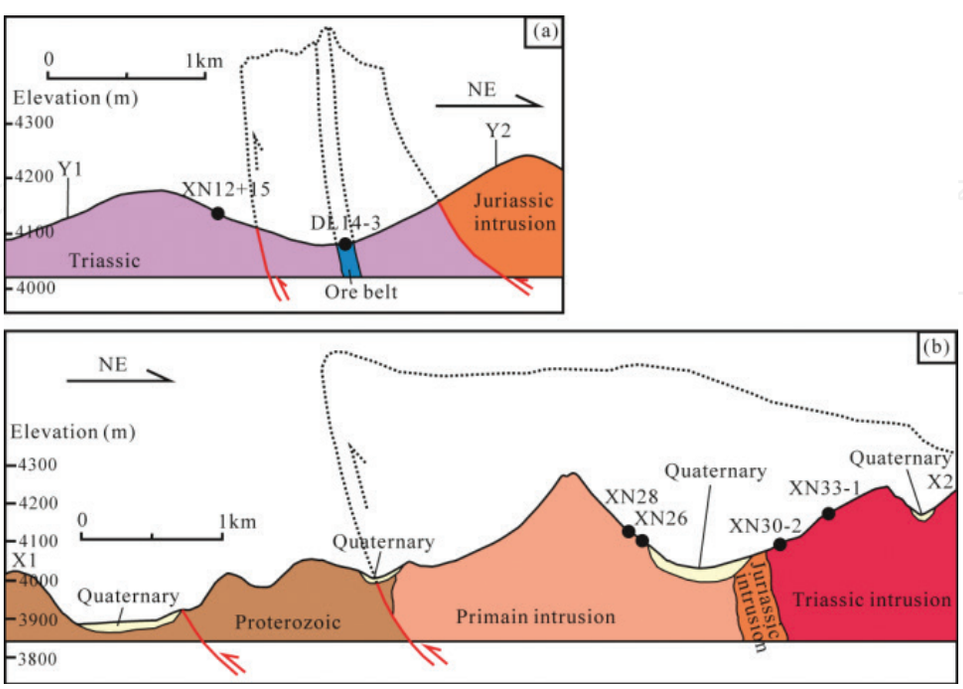

Figure 6. Cutaway views of the section Y1-Y2 (a) and section X1-X2 (b) in Harizha-Halongxiuma mine area. The ideally inferred exhumed sections are shown in dash area.

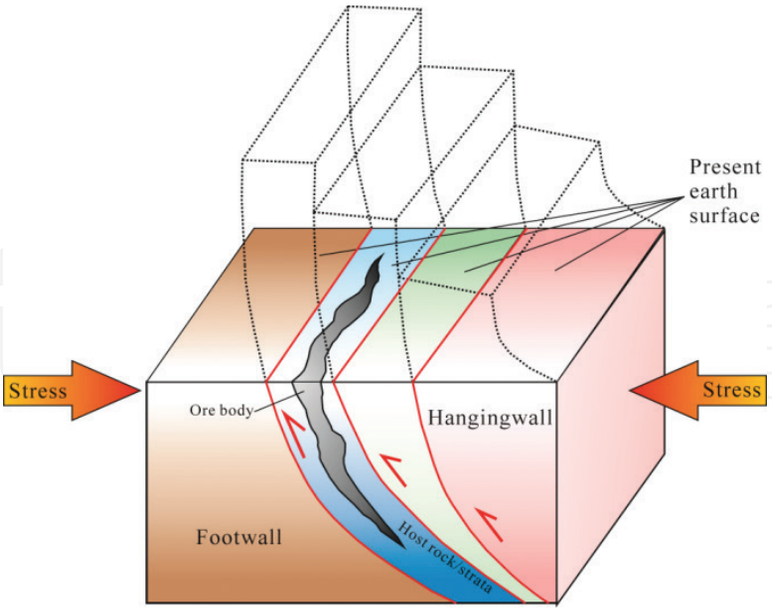

Figure 7. The ideal exhumation model for the ore bodies in compressional orogenic belt. Dash parts represent eroded stratum/intrusions/orebodies.

The analysis of exhumation history in Harizha-Halongxiuma indicates that the thrust faults in mine area exert profound influence on the preservation of ore bodies. The hangingwalls were extruded out by compression and were uplifted higher than the regional average elevation. The bulge of the Earth's surface would undergo a strong weathering process and would be eroded and exhumed rapidly. The ore bodies hosted in the hangingwall would also be eroded much more easily than that in the footwall. Thus, an ideal model is presented to outline the preservation and exhumation history of ore bodies in compressional orogenic belts (**Figure 7**). As shown in **Figure 7**, the collisions and matching between continental blocks exert compressional stress in mine areas and resulted in the development of thrust faults. The convergency between the hangingwalls and the footwalls would lead to the continuous extrusion of hangingwalls, which would result in the uplift of hangingwalls. The subsequent weathering on the bulge of the Earth's surface would result in the high-rate uplift induced exhumation. As a result, the ore bodies formed within the host rocks/stratum would be eroded due to the subsequent strong planation. The ore bodies hosted in the footwalls would be well preserved than that hosted in the hangingwalls.

So, it could be said that Harizha-Halongxiuma ore deposit area have several characteristics:

1. Apatite fission-track ages of the samples collected from the Harizha-Halongxiuma ore deposit area were obtained as (102 ± 4)-(87 ± 6). The zircon fission-track ages are ranging from (205 ± 14) to (142 ± 7) Ma. The apatite (U-Th)/He ages range from 59 to 54 Ma.
2. Six confidently modeled thermal history diagrams were obtained, and they show similar characteristics, such as rapid cooling in approximately 200–100 and 60–0 Ma and a stable period of thermal history from 100 to 60 Ma.
3. The respective average cooling rates and inferred uplift-induced exhumation for the three stages were calculated as 1.26°C/Myr and 3.60 km for the first rapid cooling stage, 0.50°C/Myr and 0.57 km for the subsequent slow cooling stage, and 1.50°C/Myr and 2.57 km for the second rapid cooling stage.

4. The exhumation of the Harizha-Halongxiuma ore deposit area since about 230 Ma was ideally calculated as 7.82 km, and the ore deposits in the study area are considered to be partially preserved.
5. An ideal exhumation model for ore bodies in compressional orogenic belt was established [34].

6. Method summary

Strong tectonic uplifting cause the gold polymetallic metallogenic system has been subjected to intense change and reform. For example, alkali-rich porphyry type of gold ore deposits in Western Yunnan Province have multi-stage of evolution and obvious diachronism, and go through conservation-changes of the ore bodies, such as uplifting-denudation, burying, shearing, missing, mineralizing superposition, supergene enrichment, long-distance migration, leaching, depletion, etc.

Same as mineralization, the conservation and changes of ore deposits would be the important part of mineral deposit geology. Research on the conservation and changes can deeply reveal the mineralization, evolution history, preservation condition, change factor, distribution regularity and hidden deposit, which are favorable for prospecting and xploration work.

6.1. Uplift and exhumation

The uplift and exhumation of the geologic bodies is the key factor of the affection in the preservation and the varition of the deposit. Uplift and denudation can directly lead to the formation of ore deposits, such as the Gandese batholithic zone in Tibet, with about 15Ma after uplift, along with the extension and collapsion of the earth crust, ore magma emplace and form the porphyry copper deposits [35]. More importantly, uplift and denudation is the key factors that the ore deposits can preserve after the formation of ore deposits [36, 37]. Mesozoic Tuwu copper deposits have been preserved in Xinjiang, for example, since differential upliftings occurred in Tuwu copper district and surrounding areas (north of Kanggur fracture), Tianshan Mountains, and then the denudation area changed into sedimentary area [38]. Bei Ya large gold deposits in Yunnan and Huayuan large lead-zinc mine in Hunan, have the low denudation degree and good preservation characteristics.

6.2. Research techniques and content

6.2.1. Research techniques

The principle of using fission track method to determine the geological age and radioactive isotope chronology are both on the basis of the percentage and the rate of disintegration in samples to determine the age of the geological samples.

The difference between them is that the fission track measurement is the radiation damage effect of fission, according to the number of 238 U in mineral, which comes from the spontaneous fission and fission time which is from spontaneous fission rate, that is the fission track age,

while the other method is measuring the product of the decay, that is according to the content of parent and daughter isotopes and the maternal isotopes decay rate, and determine the length of the decay time.

Different minerals have different fission closure temperature. The commonly used minerals in fission track are apatite, zircon and SPAR. The apatite is about 110°C [39, 40], and the zircon is 250°C [41, 42] and the SPAR is 340°C [43, 44]. The thermal evolution of different minerals in different minerals in the same mine belt can obtain the thermal evolution process of higher temperature. Hydrothermal deposit metal mineralization mainly occurs in the high temperature (350–250°C), which in the formation of quartz-sericitization, and low temperature (250–150°C) that in the formation stage of altered minerals such as kaolinization and montmorillonite, propylitization, so the fission track age of the zircon and sphene can represent metallogenic epoch. It is certainly better to combine the methods of the ^{40}Ar-^{39}Ar thermochronology, the zircon U–Pb chronology, (U-Th)/He thermochronology, and the age of the res-os.

Anyhow, basen on geological characteristics and application of a variety of thermochronology methods, we quantitatively study the uplifting-denudation and exhumation histories of the each ore districts and ore belts in Jiage, inteprete the preservation and change conditions of different ore deposits, and provide evidence for regional metallogenic potential evaluation and deep prospecting prediction.

6.2.2. Research content

1. The basic geological study
2. The reasonable sampling system
3. Thermochronology test analysis
4. Quantitative study of uplift and exhumation
5. To establish the environment model and the prospecting forecast for ore deposits

6.3. Technical solution

1. Research area selection
2. Basic geological research
3. Sample collection
4. Single mineral separation
5. Thermochronology tests
6. Geological history simulation
7. Cooling rate

Another way is by using the formula, the cooling rate Cr:

$$Cr(^{\circ}C/Ma{-}1) = (Tm - Tsurf)/tm \quad (3)$$

Tm is the closure temperature of the mineral fission track, Tsurf is the temperature of the Earth's surface and tm is the age of the surface sample.

8. The uplift rate and uplift amplitude.

$$U = D + \triangle H + \triangle s.l. \quad (4)$$

The D is the denudation, and $\triangle$H is the change in height, and $\triangle$s.l. is the magnitude of sea level change.

The rise of the rock can also be expressed as:

$$U = \text{Surface Uplift} + \text{Erosion} \quad (5)$$

The "Surface Uplift" can be described as $\triangle$E, or "Exhumation". This way, the Earth's surface increases by the same amount as u-$\triangle$E. The relationship between the rise of the rock and the rise of the Earth's surface can be learned.

9. The rate of erosion.

Denudation is the degree of erosion of surface rock caused by erosion or tectonic action. Erosion causes sustained cooling, so there is an erosion rate:

$$\text{Denudation rate} = \text{cooling rate}/\text{geothermal gradient} \quad (6)$$

Second, the temperature gradient (Q/k) is calculated based on regional heat flux (Q) and heat conduction coefficient (k). The third is to collect data that have been obtained from previous generations. It is important to note that the geothermal gradient is a regional concept. Using the sample's age and elevation drawing diagram, if the correlation is better, it can reflect the denudation rate; therefore, it can be calculated at different stages of denudation rate.

For low-temperature thermochronology, especially (U-Th)/He method, topography and wavelength, hypsography, terrain elevation difference on the surface of isothermal surface are the influencing factors; among them, the main influence is wavelength and terrain. For this reason, the denudation rate of the request can be adjusted according to the 2D model of temperature stability distribution.

10. Denudation amount

The average denudation ($\triangle$E) can be calculated based on the following formula:

$$\triangle E = (110 \pm 10^{\circ}C - Ts)/G + d \quad (7)$$

Ts is the ancient land surface temperature, G represents the paleogeothermal gradient, d is for fission track annealing with the bottom elevation and the surface elevation difference (d = fission track annealing with elevation − now at the bottom of the surface elevation).

The denudation can be calculated based on the rate of erosion and duration. In a certain period of time, its formula is as follows:

$$D = (TB - TO)/G \tag{8}$$

where D is the thickness of strata denudation (km), TB simulate the ancient temperature (°C), which corresponds the starting point for rapid cooling event, the temperature of the heat is the historical turning point, TO represent the fast cooling events at the end of the ancient temperature (°C) and G is on behalf of the geothermal gradient (°C/km).

11. Comprehensive analysis of uplift and exhumation.

Combining various quantitative data and qualitative data with the actual geological characteristics of the area, it is found that the period of metallogenic stage, the period of tectonic activity and the relation between the two are closely related; systematically, it summarizes the cooling rate of different mining areas, different parts, different time periods, the rate of growth, the rate of increase, the rate of denudation, denudation and total denudation. The evolution pattern of cooling, rising and denudation of the zone is revealed, and the evolution pattern of metallogenic and metallogenic is proposed.

12. Deposit conservation and change.

The formation depth of the deposit in the zone and the degree of denudation of the various ore deposits are obtained. The relationship between the depth and the denudation of the mineralization was summarized, and the whole process of the formation of different ore districts (beds) was probed. We identify various evolution regularities, establish the preservation-change models of the ore deposits and predict concealed ore deposits in different locations of different ore districts.

In a word, by studying a lot of hot chronology data is available, and explore the metallogenic period of time, tectonic activity and the relationship between the two, find out the mineralization and metallogenic after preservation changes during uplift denuding conditions, quantitative give the uplift rate of mining area, different sections and the main ore deposit, uplifting amplitude and stripped, reveal the regularity of mineralization and metallogenic after preservation changes during evolution and history, to set up new ore deposit geology—preserve the environment model, predict different mining area, the different locations of concealed ore deposits can be output depth, and give deposit which may have had been denudated to its extent [45].

Author details

Wanming Yuan* and Ke Wang

*Address all correspondence to: ywm010@yahoo.com

Institute of Earth Science, The China University of Geosciences, Beijing, China

References

[1] Wanming Y, Xuanxue M, Aikui Z, et al. Fission track thermochronology evidence for multiple periods of mineralization in the Wulonggou gold deposits, eastern Kunlun Mountains, Qinghai Province. Journal of Earth Science. 2013;**24**(4):471-478

[2] Silk ECH, Barnes RS. Examination of fission fragment tracks with an electron microscope. Philosophical Magazine. 1959;**4**:970-972

[3] Price PB, Walker RM. Chemical etching of charged-particle tracks in solids. Journal of Applied Physics. 1962;**33**:3407-3412

[4] Price PB, Walker RM. Observation of fossil particle tracks in natural mica. Nature. 1962; **196**:732-734

[5] Fleischer RL, Price PB. Glass dating by fission fragment tracks. Journal of Geophysical Research. 1964;**69**:331-339

[6] Fleischer RL, Price PB, Walker RM. Effects of temperature, pressure and ionization on the formation and stability of fission tracks in minerals and glasses. Journal of Geophysical Research. 1965;**70**:1497-1502

[7] Guo S, Wanming Y, Baoliu C, et al. Track fading and its applications in archaeology, tectonics and geothermal chronology in China. Journal of Earth Science. 2013;**24**(4):645-651

[8] Kang TS, Wang SC. The Fission Track Analysis Method in the Study of Geothermal Histories. Beijing: Science Press; 1991 (in Chinese)

[9] Yang T, Jianxiang Z, Wanming Y, et al. Proofs on feasibility of measuring geologic age by a thermal analysis method. International Journal of Environmental Science. 2016;**1**:97-105

[10] Jiang Y, Chang H. Apatite(U-Th)/He dating a review. Acta Petrologica et Mineralogica. 2012;**31**(5):757-766 (in Chinese)

[11] Chang Y, Xu CH, Zhou ZY. (U-Th)/He dating method: α-ejection influence and correction. Advances in Earth Science. 2010;**25**(4):418-427 (in Chinese)

[12] Xu CH, Zhou ZY, Chang Y. Genesis of Daba arcuate structural belt related to adjacent basement upheavals: Constraints from fission-track and (U-Th)/He thermochronology. Science China Earth Sciences. 2010;**40**(12):1684-1696 (in Chinese)

[13] Yang TS. Feasibility of probing solid state nuclear tracks by thermal analysis method. Chinese Science Bulletin. 2007;**52**(4):380-383 (in Chinese)

[14] Yang TS, He SR, Li TX, et al. Measurement of solid state nuclear tracks in apatite by thermal analysis method. Chinese Science Bulletin. 2009;**54**(17):2495-2499 (in Chinese)

[15] Yang TS, Shi YQ, Li YG, Wang DW, et al. Research program of determination of geological age by thermal analysis method. Journal of Earth Science. 2013;**24**(4):657-662

[16] Bellemans F, De Corte F, Van Den Haute P. Composition of SRM and CN U-doped glasses: Significance for their use as thermal neutronfluence monitors in fission track dating. Radiation Measurements. 1994;**24**(2):153-160

[17] Hurford AJ, Green PF. A users'guide to fission-track dating calibration. Earth and Planetary Science Letters. 1982;**59**:343-354

[18] Hurford AJ. Standardization of fission track dating calibration: Recommendation by the fission-track working group of the I.U.G.S. subcommission on geochronology. Chemical Geology. 1990;**80**:171-178

[19] Galbraith RF. On statistical models for fission track counts. Mathematical Geology. 1981; **13**:471-488

[20] Yuan W, Bao Z, Dong J, et al. Zircon and apatite fission track analyses on mineralization ages and tectonic activities of Tuwu-Yandong porphyry copper deposit in northern Xinjiang, China. Science in China Series D: Earth Sciences. 2007;**50**(12):1787-1795

[21] Green PF, Duddy IR, Laslett GM, et al. Thermal annealing of fission tracks in apatite, 4. Quantitative modeling techniques and extensions to geological timescales. Chemical Geology. 1989;**79**:155

[22] Wanming Y, Wang S, Shengrong L, et al. Apatite fission track dating evidence on the tectonization of Gangdese block, south Qinghai-Tibetan plateau. Chinese Science Bulletin. 2002;**47**(3):240-244

[23] Yuan WM, Zhang XT, Dong JQ, et al. A new vision of the intracontinental evolution of the eastern Kunlun Mountains, Northern Qinghai-Tibet plateau, China. Radiation Measurements. 2003;**36**(2003):357-362

[24] Wanming Y, Zheng Q, Bao Z, et al. Zircon fission track thermochronology constraints on mineralization epochs in Altai Mountains, northern Xinjiang, China. Radiation Measurements. 2009;**44**(2009):950-954

[25] Copeland P, Harrison TM, Yun P. Thermal evolution of the Gangdese batholith, southern Tibet: A history of episodic unroofing. Tectonics. 1995;**14**:223-236

[26] Harrison TM, Copeland P, Kidd WSF. Activation of the Nyainqentanghla shear zone: Implications for uplift of the southern Tibet plateau. Tectonics. 1995;**14**:658-676

[27] Yuan Wanming, Hou Zhengqian, Li Shengrong, et al. Fission track evidence on thermal history of Jiama polymetallic ore district, Tibet. Science in China (Series D), 2001; **44**(Sup):139-145

[28] Wanming Y, Bao Z, Dong J, et al. Zircon and apatite fission track analyses on mineralization ages and tectonic activities of Tuwu-Yandong porphyry copper deposit in northern Xinjiang, China. Science in China (Series D). 2007;**50**(12):1787-1795

[29] Deng Jun, Yuan Wanming, Emmanuel John Muico Carranza, et al. Geochronology and thermochronometry of the Jiapigou gold belt, northeastern China: New evidence for multiple episodes of mineralization. Journal of Asian Earth Sciences. 2014;**89**:10-27

[30] Ketchma RA. Forward and inverse modeling of low-temperature thermochronometry data. Review in Mineralogy and Geochemistry. 2005;**58**(1):275-314

[31] Ketchman RA, Carter A, Donelick RA, Barbarand J, Hurford AJ. Improved measurement of fission-track annealing in apatite using c-axis projection. American Mineralogist. 2007; **92**:789-798

[32] Ketchman RA, Carter A, Donelick RA, Barbarand J, Hurford AJ. Improved measurement of fission-track annealing in apatite. American Mineralogist. 2007;**92**:799-810

[33] Xu QL. Study on Metallogenesis of Porphyry Deposit in Eastern Kunlun Orogenic Belt, Qinghai Province. Changchun, China: Department of Earth Sciences, Jilin University; 2014 (in Chinese)

[34] Feng YL, Yuan WM, Tian YT, et al. Preservation and exhumation history of the Harizha-Halongxiuma mining area in the East Kunlun Range, Northeastern Tibetan Plateau, China. Ore Geology Reviews 2017;**84**:116-133

[35] Qu XM, Hou ZQ, Khin Z, Mo XX, Xu WY, Xin HB. A large-scale copper ore-forming event accompanying rapid uplift of the southern Tibetan plateau: Evidence from zircon SHRIMP U–Pb dating and LA ICP-MS analysis. Ore Geology Reviews. 2009;**36**(1-3):52-64

[36] Márton I, Moritz R, Spikings R. Application of low-temperature thermochronology to hydrothermal ore deposits: Formation, preservation and exhumation of epithermal gold systems from the eastern Rhodopes, Bulgaria. Tectonophysics. 2010;**483**(3-4):240-254

[37] Schardt C, Large RR. New insights into the genesis of volcanic-hosted massive sulfide deposits on the seafloor from numerical modeling studies. Ore Geology Reviews. 2009;**35**(3-4):333-351

[38] Wu ZN, Huang JH, Yu SP, Muhtar ZR, Yang XR, Dili XT, Han WQ. Paleogeographic environment for reserving and forming of Tuwu deposit in eastern Tianshan Mountains, Xinjiang. Arid Land Geography. 2007;**30**(2):189-195 (in Chinese)

[39] Gleadow AJW, Duddy IR. A natural long-term track annealing experiment for apatite. Nuclear Tracks. 1981;**5**:169-174

[40] Kemp PJJ. Fission track analysis reveals character of collisional tectonics. Tectonics. 1989;**8**(2):169-195

[41] Yamada R, Tagami T, Nishimura S, Ito H. Anealing kinetics of fission tracks in zircon: An experimental study. Chemical Geology (Isotope Geoscience Section). 1995;**122**:249-258

[42] Wagner GA, Haute PVD. Fission track dating. Ferdinand Enke Verlag, Stuttgart. 1992:95-119

[43] Nagpaul KK. Fission track geochronology of India. In: Goswami JN, editor. Nuclear Tracks. Bangalore: India Academy of Sciences; 1982. pp. 53-65

[44] Gleadow AJW, Lovering JF. Geometry factor for external detectors in fission track dating. Nuclear Track Detection. 1977;**1**:99-106

[45] Yuan WM. Thermochronological method of revealing conservation and changes of mineral deposits. Acta Petrologica Sinica. 2016;**32**(8):2571-2578